Applied Physics Letters

Mobility spectrum analysis on three-dimensional topological insulator $BiSbTeSe_2$

Cite as: Appl. Phys. Lett. **118**, 253107 (2021); https://doi.org/10.1063/5.0047773
Submitted: 16 February 2021 . Accepted: 04 June 2021 . Published Online: 23 June 2021

Jimin Wang, Alexander Kurzendorfer, Lin Chen, Zhiwei Wang, Yoichi Ando, Yang Xu, Ireneusz Miotkowski, Yong P. Chen, and Dieter Weiss

Applied Physics Letters ARTICLE scitation.org/journal/apl

Mobility spectrum analysis on three-dimensional topological insulator $BiSbTeSe_2$

Cite as: Appl. Phys. Lett. **118**, 253107 (2021); doi: 10.1063/5.0047773
Submitted: 16 February 2021 · Accepted: 4 June 2021 ·
Published Online: 23 June 2021

View Online Export Citation CrossMark

Jimin Wang,[1,a)] Alexander Kurzendorfer,[1] Lin Chen,[1] Zhiwei Wang,[2,3] Yoichi Ando,[2] Yang Xu,[4] Ireneusz Miotkowski,[4] Yong P. Chen,[4,5,6,7,8,9] and Dieter Weiss[1,a)]

AFFILIATIONS

[1]Institute of Experimental and Applied Physics, University of Regensburg, 93040 Regensburg, Germany
[2]Physics Institute II, University of Cologne, Zülpicher Str. 77, 50937 Köln, Germany
[3]Centre for Quantum Physics, Key laboratory of advanced optoelectronic quantum architecture and measurement (MOE), School of Physics, Beijing Institute of Technology, Beijing, 100081, China
[4]Department of Physics and Astronomy, Purdue University, West Lafayette, Indiana 47907, USA
[5]School of Electrical and Computer Engineering and Birck Nanotechnology Center, Purdue University, West Lafayette, Indiana 47907, USA
[6]Purdue Quantum Science and Engineering Institute, Purdue University, West Lafayette, Indiana 47907, USA
[7]WPI-AIMR International Research Center for Materials Sciences, Tohoku University, Sendai 980-8577, Japan
[8]Institute of Physics and Astronomy, Aarhus University, 8000 Aarhus-C, Denmark
[9]Institute of Physics and Astronomy and Villum Center for Hybrid Quantum Materials and Devices, Aarhus University, 8000 Aarhus-C, Denmark

[a)]**Authors to whom correspondence should be addressed:** jimin.wang@physik.uni-regensburg.de and dieter.weiss@physik.uni-regensburg.de

ABSTRACT

We conducted mobility spectrum analysis on a high quality three dimensional topological insulator film of $BiSbTeSe_2$ to extract mobility μ and carrier density n. Top and bottom gates were applied to tune the carrier density on top and bottom surfaces independently. At 1.5 K, when the conduction is entirely dominated by the Dirac surface states, we always find two dominant conduction channels (top and bottom surfaces), with $\mu = 500$–$3000\ \mathrm{cm^2/(V\,s)}$ and n on the order of $10^{12}\ \mathrm{cm^{-2}}$. However, at sufficiently high temperature ($T = 85$ K), when the bulk contributes, a third channel with maximum mobility $\mu \sim 400\ \mathrm{cm^2/(V\,s)}$ and n on the order of 10^{11}–$10^{13}\ \mathrm{cm^{-2}}$ opens. Our data show the feasibility of the method to analyze the different conduction channels in a topological insulator, being also promising for other similar material systems.

Topological insulators (TIs) feature insulating bulk and metallic Dirac surface conduction.[1–4] This peculiar property has triggered a vast amount of research activities, due to the interesting fundamental physics, and potential applications in spintronics, quantum computing, and the next generation storage media.[2,5–8] However, TIs have been plagued by the unintentional intrinsic doping, which shifts the Fermi level to the conduction or valence band and results in bulk conduction. Therefore, the resulting conductivity is usually a mixture of both surface and the bulk contributions.[9] Efforts have been made to compensate doping—i.e., combining n- and p-doped TIs—and to pin the Fermi level in the bandgap, which enable dominating or even pure surface conduction. There are several successful examples, such as $(Bi_{1-x}Sb_x)_2Te_3$ and $Bi_{1-x}Sb_xTe_{1-y}Se_y$.[10–14] Nevertheless, even for these TIs, multichannel conduction still occurs. For example, in three-dimensional (3D) TI thin films with vanishing bulk conduction, top and bottom surfaces provide two individual channels, whose mobility and carrier density can be tuned independently.

To obtain the conduction parameters of the individual channel in a material, i.e., carrier type, mobility (μ), and carrier concentration (n), there are discussions on two-band model, which is applicable for two channels.[15,16] However, for multiple channels (more than two), the method is incapable to manage so many fitting parameters. Here,

we apply an easy to use method—mobility spectrum analysis (MSA)—in the high quality compensated TI $BiSbTeSe_2$ (BSTS). The method relies on Hall and resistivity data taken at different out-of-plane magnetic fields. A generalized theory and test analysis on composed data are in the supplementary material; and the detailed theory, together with some examples of semiconductors with multichannel conduction, can be found in Ref. 17. Further discussions on the method and a few successful implementations on other material systems, multilayers, and superlattices suggest the feasibility of the method.[18–21]

So far the method has not been used to analyze any TI. In our discussion below, we focus on devices with both top and bottom gates, such that the property of an individual surface can be tuned. The analysis for BSTS shows that there are two dominating conduction channels at cryogenic temperatures—the two surface channels—and an emerging third one—the bulk conduction channel—with the increasing temperature.

The analysis assumes that the conduction is pure Drude-like and isotropic, and the total conductivity tensor components are given by the sum of all the conduction channels in the form, $\sigma_{xx}(B) = \int \frac{s(\mu)d\mu}{1+\mu^2B^2}$, and $\sigma_{xy}(B) = \int \frac{\mu Bs(\mu)d\mu}{1+\mu^2B^2}$, with B the magnetic field, μ the mobility, and $s(\mu)$ the conductivity density function.[17] The mobility μ is defined as positive for holes and negative for electrons. By varying μ, one gets plots of the maximum possible conductivity (σ_{max})-μ and the maximum possible carrier density (n_{max})-μ with one or more peaks, from which the individual channel information is then extracted.

In our experiments we used high quality BSTS single crystals,[13,14] exfoliated using scotch tape onto highly p-doped silicon chips, coated with 285 nm SiO_2. The doped Si serves as back gate (back gate voltage: V_{bg}). The 10 nm Ti and 100 nm Au, deposited by electron beam evaporation and thermal evaporation, form Ohmic contacts. A thin layer of h-BN was then transferred on top of BSTS, serving as both encapsulation and gate insulator. Furthermore, 10 nm Ti and 100 nm Au layers were deposited as gate electrode to which the top gate voltage (V_{tg}) is applied. Transport measurements were carried out either in a dilution refrigerator at $T = 50$ mK or in a ^{4}He cryostat above $T = 1.5$ K. B, up to 14 T, is applied perpendicular to the sample plane.

An optical image of one of the devices is shown in the upper inset of Fig. 1(a). Similar results were obtained on several different devices. Below we focus on one of them, using BSTS material from Cologne.[13] Data of BSTS material from Purdue[14] can be found in the supplementary material.

The temperature dependence of the resistivity $\rho_{xx}(T)$ of the BSTS device with both gates grounded [see Fig. 1(a)] displays two distinct regions: above ~65 K, the temperature dependence of $\rho_{xx}(T)$ is bulk dominated, indicated by an increasing $\rho_{xx}(T)$ with the decreasing T, as in semiconductors. Below ~65 K, the T-dependence is determined by the surface channels and metallic conductivity ($\rho_{xx}(T)$ decreases with the decreasing T) prevails. To cover the two regimes, we focused on three temperatures (1.5, 40, and 85 K), marked by colored points in Fig. 1(a).

The thickness of the BSTS flake is about 67 nm, which enables independent tuning of top and bottom surfaces across the charge neutrality point (CNP). It is also supported by the nearly vertical and horizontal dashed lines in the quantum Hall effect gate mapping at $B = 14$ T in Fig. 1(b). Thus, the carrier type on top and bottom surface can be tuned the same (nn, or pp, the former letter represents the top surface carrier type, and latter one the bottom surface) or opposite polarity (pn, or np). An example of $\rho_{xx} - B$ and $\rho_{xy} - B$ traces with lower B only up to 9 T for the pn regime ($V_{tg} = -5$ V and $V_{bg} = 25$ V) at different temperatures is presented in Fig. 1(c). At low T (e.g., 1.5 K), the weak antilocalization (WAL) effect causes a dip near zero B, which vanishes with the increasing T. At $T = 85$ K, WAL disappears completely. As our MSA assumes Drude-like transport, we fit the low field region, in which WAL prevails, with a parabolic fit as shown by the dashed lines for $T = 1.5$ K and $T = 40$ K traces in Fig. 1(c). The approximation does not affect the data at higher B, but only smooths the data close to zero B. No such approximation is needed for $T = 85$ K. The $\rho_{xy} - B$ traces were not affected by the WAL effect, yet a strong nonlinearity was observed. This is especially pronounced when the carrier type on top and bottom surface is different.

For the MSA, datasets of (B, σ_{xx} and σ_{xy}) taken at different B-values are used as input. At first sight, the largest possible number of datasets seems desirable; however, they are limited to 7 by the

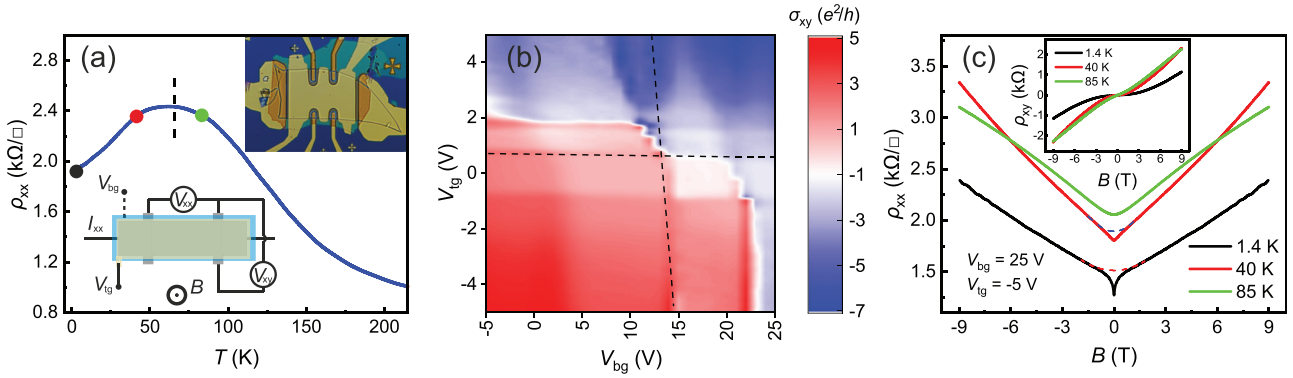

FIG. 1. Transport data. (a) Resistivity–temperature relation, showing a transition from a typical semiconductor T-dependence (above ~65 K) to a metallic one (below ~65 K). The top-right inset is an optical micrograph of the device and the bottom inset shows the measurement setup. (b) σ_{xy} mapping at $B = 14$ T and $T = 50$ mK, when both V_{tg} and V_{bg} are varied. Dashed lines show the charge neutrality points of top and bottom gates, respectively. The fact that these lines are nearly horizontal/vertical means that the two layers can be tuned independently. (c) $\rho_{xx} - B$ traces at $V_{tg} = -5$ V, $V_{bg} = 25$ V, and at three temperatures, 1.5, 40, and 85 K, respectively. Dashed lines are parabolic fits by removing the WAL effect dip (non-Drude type) near zero B. The inset shows the corresponding $\rho_{xy} - B$ traces.

accumulated round-off errors in the large matrix calculation that will invalidate the method.[17] σ_{xx} and σ_{xy} can be obtained from the inverse of the resistivity tensor: $\sigma_{xx} = \frac{\rho_{xx}}{\rho_{xx}^2+\rho_{xy}^2}$ and $\sigma_{xy} = \frac{\rho_{xy}}{\rho_{xx}^2+\rho_{xy}^2}$. The minimum and maximum B-values were 0 and 9 T, respectively. Then, we choose a value B_0 and 4 Bs, which are equidistantly spaced between 1/9 T^{-1} and $1/B_0$ to obtain equal resolution at high and low mobilities. In addition, to minimize effects, which result from the limited number of data points, we average the MSA results over five data point configurations with $B_0 = 1$, 1.5, 2, 2.5, and 3 T, respectively.

Figure 2 shows the MSA results at $T = 1.5$ K, where pairs of the generated $\sigma_{max} - \mu$ (top panels) and $n_{max} - \mu$ (bottom panels) relations are presented. All analyses show peaks in $\mu \in$ (–6000, 6000) $cm^2/(V\,s)$ for the different combinations of V_{tg} and V_{bg}. The peaks at $\mu > 0$ are blue-colored, representing holes, while the red peaks at $\mu < 0$ represent electrons. As long as there is a dominating conduction channel with mobility μ_0, peaks at μ_0 will be obtained. In Fig. 2(a), V_{bg} was fixed at 25 V, and V_{tg} was varied in steps from 5 to –5 V. At V_{tg} = –5 V, two dominant peaks were observed, indicating two dominant conduction channels: electrons and holes on the bottom and top surfaces, respectively. As explained above, the sample is in the *pn* regime. However, the situation changes when V_{tg} is gradually increased to positive values. The peak on the hole side shrinks and almost vanishes at $V_{tg} = 5$ V, when the top surface becomes *n*-type (*nn* regime). Since the two surfaces are with similar μ and n, the two conduction channels appear as a single one (red peak). Thus, only one peak prevails. The corresponding $n_{max} = |\sigma_{max}/\mu q|$ is shown in Fig. 2(d), where $q = -e$ and e for electrons and holes, respectively. The results close to zero μ were omitted (owing to division by zero). Comparing with Fig. 2(a), the peak positions are almost the same. Thus, $\sigma_{max} - \mu$ and $n_{max} - \mu$ plots provide the same information.

The situation is similar if the bottom surface is fixed to be hole type ($V_{bg} = -25$ V). As demonstrated in Fig. 2(b), the dominating one peak at $V_{tg} = -5$ V (*pp* regime) gradually evolves into two equally high peaks at $V_{tg} = 5$ V (*np* regime). The corresponding n_{max} is shown in Fig. 2(e).

Figures 2(c) and 2(f) show results where now V_{tg} is fixed and V_{bg} is varied. At fixed $V_{tg} = 5$ V and the top surface is *n*-type. By varying V_{bg}, one also observes, as expected, a single dominant peak at V_{bg} = 25 V (*nn* regime), and two dominant peaks at $V_{bg} = -25$ V (*np* regime). The evolution of n_{max} is also consistent with σ_{max}, showing a similar peak structure.

At 85 K, the WAL dip vanishes and bulk conduction contributes, too. To compare with the 1.5 K data, we show in Fig. 3 the same V_{bg} and V_{tg} settings as in Fig. 2. In Fig. 3(a), V_{bg} is fixed at 25 V. While as before at 1.5 K electron and/or hole peaks of surface carriers dominate the spectrum, a smaller peak close to zero mobility appears for all V_{tg}. This extra peak seems not to belong to any of the surface channels, and we ascribe it to bulk carriers. In most cases, the peaks are on the (blue) hole side but sometimes also on the electron side [see $V_{tg} = 3$ and 5 V in Fig. 3(a)]. This scatter around $\mu = 0$ is due to the accuracy of the method, as the peak is so close to 0 [maximum value of $\mu \sim 400\,cm^2/(V\,s)$]. Such values of bulk mobility in BSTS were also reported by others.[10,12] In addition, the typical n is on the order of

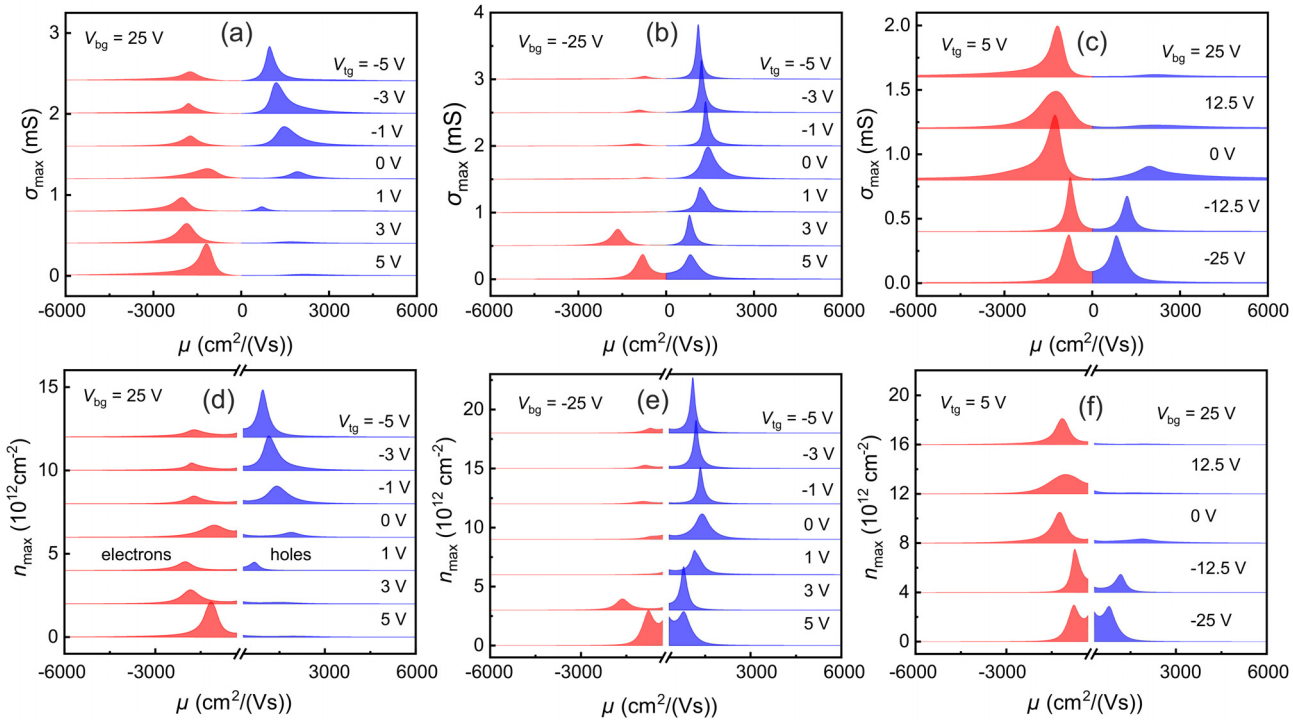

FIG. 2. MSA at $T = 1.5$ K. (a) $\sigma_{max} - \mu$ relation at fixed $V_{bg} = 25$ V, V_{tg} is varied from 5 V to −5 V. Each curve is shifted by 0.4 mS for clarity. (b) $\sigma_{max} - \mu$ relation at fixed $V_{bg} = -25$ V, and varying V_{tg}. The curves are shifted by 0.5 mS for clarity. (c)$\sigma_{max} - \mu$ relation at fixed $V_{tg} = 5$ V. V_{bg} is varied from 25 to −25 V in step of 12.5 V. Each trace is shifted by 0.4 mS. (d)–(f) are the corresponding $n_{max} - \mu$ in (a)–(c), shifted by 2×10^{12}, 3×10^{12}, 4×10^{12} cm^{-2}, respectively. Here the peak heights, rather than the area, provide information on σ_{max} and n_{max}.

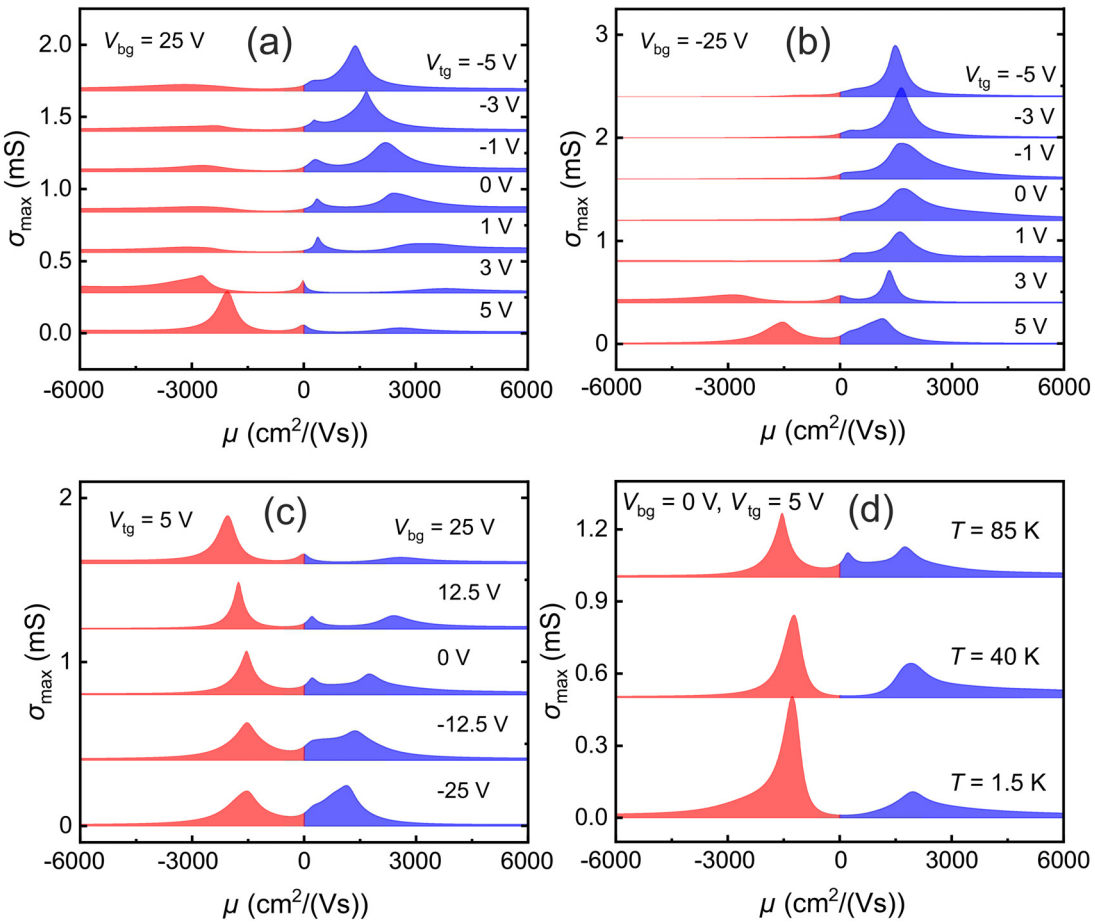

FIG. 3. MSA at elevated temperatures. (a)–(c) $\sigma_{max} - \mu$ relation at $T = 85$ K at fixed $V_{bg} = 25$ V (a) and $V_{bg} = -25$ V (b), while V_{tg} is varied from 5 to −5 V; and fixed $V_{tg} = 5$ V (c), while V_{bg} is varied from −25 to 25 V. (d) $\sigma_{max} - \mu$ relation at fixed $V_{bg} = 0$ and $V_{tg} = 5$ V at different temperatures. All curves are shifted for clarity by 0.28 mS (a), 0.4 mS (b) and (c), 0.5 mS (d), respectively.

10^{12} cm^{-2}, which is comparable with the one of the surface states. [n_{max} is calculated from $\sigma_{max}/|\mu q|$, using the peak conductivity at the bulk peak position, as shown in Fig. 3(d). The $n_{max} - \mu$ plots are not shown, as the corresponding peaks are covered by the 0–μ peaks (divided by 0).]

The situation is almost the same when V_{bg} is fixed to another value, for example, −25 V [Fig. 3(b)]. In addition, by fixing V_{tg} instead, for example, at 5 V [Fig. 3(c)], we obtain similar results. At $V_{bg} = -25$ V, the two dominating peaks stem from the two surface channels. The bulk channel is indicated by a shoulder in the finite signal around $\mu \sim 0$. With the decreasing V_{bg}, the peak on the hole side becomes weaker. In summary, there are three main differences compared to the 1.5 K case: (i) around $\mu \sim 0$, a mobility peak remains reflecting the existence of bulk carriers at elevated T. (ii) All the peaks away from zero mobility are more broadened. (iii) Unlike for $T = 1.5$ K and $V_{bg} = 25$ V, where the peak on the hole side almost vanishes in the nn regime (i.e., for $V_{tg} = 5$ V), the peak on the hole side becomes only weaker at $T = 85$ K but does not vanish. The reason might be related to the compensated doping of BSTS, allowing electrons and holes, populated by the thermal excitation, to coexist at elevated temperatures.

Apart from $T = 1.5$ K and $T = 85$ K, we also carried out the MSA using data taken at an intermediate temperature $T = 40$ K. Figure 3(d) shows the temperature dependence of the mobility spectrum for fixed $V_{bg} = 0$ V and $V_{tg} = 5$ V. While, at 1.5 and 40 K, two peaks dominate the spectrum, a third one emerges at low mobilities at $T = 85$ K. In general, the results at $T = 40$ K are closer to the $T = 1.5$ K data. This is in line with a still nonactivated bulk conduction.

Figure 4 summarizes the μ and n_{max} data extracted for different V_{tg} and V_{bg} voltages at low and high temperatures, respectively. At $T = 1.5$ K [Figs. 4(a) and 4(b)], two dominating conduction channels can be identified, i.e., top and bottom surfaces. The mobility is in the range of $\mu = 500$–3000 cm^2/(V s), and the maximum carrier density for electrons and holes is on the order of 10^{11}–10^{13} cm^{-2}, depending on the gate voltages. These two surface transport channels are also present at $T = 85$ K [Figs. 4(c) and 4(d)], with similar mobility and carrier density at $T = 1.5$ K. In addition, a third conduction channel appears, ascribed to bulk conduction. The mobility of the bulk is

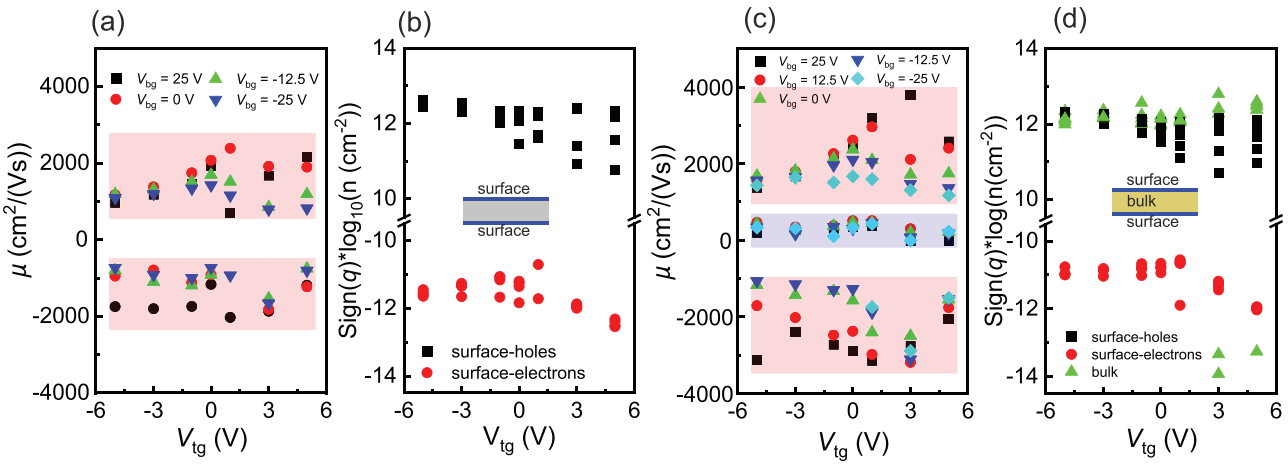

FIG. 4. Overview of the mobility and carrier density. (a) μ–V_{tg} relation for different V_{bg} at $T = 1.5$ K. (b) n_{max}–V_{tg} in log scale for different V_{bg} at $T = 1.5$ K. Positive (negative) values represent holes (electrons). The inset sketches the two surface conduction channels. (c) μ–V_{tg} relation for different V_{bg} at $T = 85$ K. (b) n_{max}–V_{tg} in log scale for different V_{bg} at $T = 85$ K. The inset sketches the two-surface conduction channels and the bulk channel.

significantly lower, with the maximum values of the mobility $\mu \sim 400\ \mathrm{cm}^2/(\mathrm{Vs})$. However, the maximum carrier density calculated from $\sigma_{max}/|\mu q|$ is on the same order compared to that of the surface states (in units of cm^{-2}).

Ideally, MSA would generate sharp discrete peaks (see the analysis on composed data in the supplementary material, and example in Ref. 17). However, the spectra we obtain for BSTS from our analysis are not ideal but significantly broadened. Several factors can cause broadening: nonideal geometric Hall bar shape, measurement (voltage, magnetic field, current, etc.) errors, material inhomogeneity, the assumption of pure Drude-like conduction, and the approximation of an isotropic band structure.[17] In addition, the distribution of mobility/relaxation time in each channel can cause broadening, too. Nevertheless, the data show that MSA is a useful technique to get information on the different bulk and surface conduction channels in BSTS.

In summary, we conducted the mobility spectrum analysis on BSTS, a 3D-TI, using magnetotransport data. At $T = 1.5$ K, one or two prominent peaks in $\sigma_{max} - \mu$ plots indicate unipolar or bipolar surface conduction channels, respectively. At an elevated temperature of 85 K, a third peak emerges at low mobility values which we assign to the bulk conduction channel. Our analysis shows the feasibility of the method to extract important information, such as mobility and carrier density in 3D topological insulators.

See the supplementary material for the general theory of the mobility spectrum analysis method; the test analysis on composed data; and transport properties and mobility spectrum analysis on the Purdue BSTS samples.

The work at Regensburg was funded by the Deutsche Forschungsgemeinschaft (DFG, German Research Foundation)-Project-ID 314695032-CRC 1277 (Subprojects A07, A08). This project has received further funding from the European Research Council (ERC) under the European Union's Horizon 2020 research and innovation programme (Grant Agreement No. 787515, ProMotion), as well as the Alexander von Humboldt Foundation. The work at Cologne was funded by the Deutsche Forschungsgemeinschaft (DFG, German Research Foundation)-Project No. 277146847-CRC 1238 (Subproject A04). The Purdue team acknowledges partial support of the TI growth and characterization work by DARPA MESO program (Grant No. N66001-11-1-4107) and by NSF (Grant Nos. DMR1410942 and EFMA-1641101).

DATA AVAILABILITY

The data that support the findings of this study are available from the corresponding authors upon reasonable request.

REFERENCES

[1]M. Z. Hasan and C. L. Kane, Rev. Mod. Phys. **82**, 3045 (2010).
[2]Y. Ando, J. Phys. Soc. Jpn. **82**, 102001 (2013).
[3]L. Fu and C. L. Kane, Phys. Rev. Lett. **100**, 096407 (2008).
[4]L. Fu and C. L. Kane, Phys. Rev. B **79**, 161408(R) (2009).
[5]L. Smejkal, Y. Mokrousov, B. Yan, and A. H. MacDonald, Nat. Phys. **14**, 242 (2018).
[6]X.-L. Qi and S.-C. Zhang, Rev. Mod. Phys. **83**, 1057 (2011).
[7]J. Zhang, C. Triola, and E. Rossi, Phys. Rev. Lett. **112**, 096802 (2014).
[8]L. D. Alegria, H. Ji, N. Yao, J. J. Clarke, R. J. Cava, and J. R. Petta, Appl. Phys. Lett. **105**, 053512 (2014).
[9]J. G. Analytis, R. D. McDonald, S. C. Riggs, J.-H. Chu, G. S. Boebinger, and I. R. Fisher, Nat. Phys. **6**, 960 (2010).
[10]C. Weyrich, M. Drögeler, J. Kampmeier, M. Eschbach, G. Mussler, T. Merzenich, T. Stoica, I. E. Batov, J. Schubert, L. Plucinski, B. Beschoten, C. M. Schneider, C. Stampfer, D. Grützmacher, and T. Schäpers, J. Phys. **28**, 495501 (2016).
[11]R. Yoshimi, A. Tsukazaki, Y. Kozuka, J. Falson, K. S. Takahashi, J. G. Checkelsky, N. Nagaosa, M. Kawasaki, and Y. Tokura, Nat. Commun. **6**, 6627 (2015).
[12]J. Zhang, C.-Z. Chang, Z. Zhang, J. Wen, X. Feng, K. Li, M. Liu, K. He, L. Wang, X. Chen, Q.-K. Xue, X. Ma, and Y. Wang, Nat. Commun. **2**, 574 (2011).
[13]T. Arakane, T. Sato, S. Souma, K. Kosaka, K. Nakayama, M. Komatsu, T. Takahashi, Z. Ren, K. Segawa, and Y. Ando, Nat. Commun. **3**, 636 (2012).

[14]Y. Xu, I. Miotkowski, C. Liu, J. Tian, H. Nam, N. Alidoust, J. Hu, C.-K. Shih, M. Z. Hasan, and Y. P. Chen, Nat. Phys. **10**, 956 (2014).
[15]F. Yang, S. Ghatak, A. A. Taskin, K. Segawa, Y. Ando, M. Shiraishi, Y. Kanai, K. Matsumoto, A. Rosch, and Y. Ando, Phys. Rev. B **94**, 075304 (2016).
[16]S. Sykora, J. Schoop, L. Graf, G. Shipunov, I. V. Morozov, S. Aswartham, B. Büchner, C. Hess, R. Giraud, and J. Dufouleur, Phys. Rev. Res. **2**, 033041 (2020).
[17]W. A. Beck and J. R. Anderson, J. Appl. Phys. **62**, 541 (1987).
[18]J. Antoszewski and L. Faraone, J. Appl. Phys. **80**, 3881 (1996).
[19]J. Antoszewski, L. Faraone, I. Vurgaftman, J. R. Meyer, and C. A. Hoffman, J. Electron. Mater. **33**, 673 (2004).
[20]K. K. Huynh, Y. Tanabe, T. Urata, S. Heguri, K. Tanigaki, T. Kida, and M. Hagiwara, New J. Phys. **16**, 093062 (2014).
[21]I. Vurgaftman, J. R. Meyer, C. A. Hoffman, S. Cho, A. DiVenere, G. K. Wong, and J. B. Ketterson, J. Phys. **11**, 5157 (1999).